Scientific Research Publishing

# Validation Approach of the Tectonic Lineament Extraction Enhancement Using Sentinel 2A Images and Modified 3 × 3 Bidirectional Prewitt Filters. Case Study: Grombalia, Tunisia

## Mansouri Karim[1], Noamen Rebai[2], Sonya Gannouni[3], Slimene Sedrette[2], Imed Riadh Farah[1]

[1]ENSI, École Nationale des Sciences de l'Informatique Manouba, Manouba, Tunisia
[2]Geotechnical Engineering and Georisk Research Laboratory (LR14ES03), National School of Engineering of Tunis, University of Tunis El Manar, Tunis, Tunisia
[3]Laboratoire de Géoressources, CERTE, Technopole de Borj Cedria, Borj Cedria, Tunisia
Email: karim.mansouri@ensi-uma.tn, imed.riadh.farahgmail.com, noamen.rebai@enit.utm.tn, ssedrette@gmail.com, gannounisonia2017@gmail.com

## Abstract

In this study, filters are used to extract directional tectonic lineaments and, thus, to reveal the presence of faults or fractures in the satellite images. The extraction process consists first in eliminating other different types of lineaments (e.g. the lithological limit, ridgelines, hydrographic network, roads, etc.). Besides, a comparative and quantitative approach is applied to show that when the directional Prewitt filter has a zero setting of the opposite of the assumed direction, as is the case of the N-S direction, the East-West direction is also set to zero. This research work, based on a bidirectional filter (N-S; E-W), shows satisfactory results especially concerning the quantitative fluctuation of lineament directions by interval. This fluctuation is in perfect agreement with the lineaments provided by the digitizing of the different tectonic accidents directions extracted in a GIS environment from the geological map of Grombalia. In this research work, a quantitative approach was used to evaluate the result of the lineament extraction methodology based on one direction analysis and by an interval of directions. Indeed, the N45 lineament direction, well documented in the geological study of the region, was more clearly distinguished by applying the Prewitt filter than by using the Sobel filter. The result was validated by comparison with the results obtained by the digitization of the tectonic accidents mapped on the geological map.

Grombalia, Tunisia

## 1. Introduction

Tectonic lineament mapping facilitates the location of the appropriate site for mineral exploration [1] [2] [3]. It is also very effective in mineral prospection. Indeed, this technique allows orienting prospection during the reconnaissance phase. In hydrogeology and hydrology, many recent works ([4] [5] [6]) have shown that these fractures originated groundwater formation in fissured basement environments and constitute the ultimate zones of water flow. Thus, the investigation of this faults network during dam construction remains essential.

The main objective of this study is to improve the process of tectonic accidents lineaments extraction from optical satellite images, although this extraction could be carried out from other data sources (e.g. geomorphology and morphometric indices) as well as from other types of sensors (e.g. radar images) [7] [8].

This study uses Sentinel 2A multi-spectral optical images with a 10 m resolution and applies a two-step extraction approach.

The first step involves the tectonic accidents mapping based on a geological map constructed relying on surveys and field observations. The mapped accidents are digitized and classified in the form of an attribute database containing, essentially the orientation towards north by applying our algorithm to determine these directions in a GIS environment. The approach of quantifying the directions by unit or by interval is employed to compare with field reality. Indeed, it requires, first, digitizing the tectonic accidents mapped in a GIS environment using ArcGIS software.

It is very important to note that the access difficulties in several sectors of the studied region, because of natural obstacles (rivers, mountains, dense forests, and more often the large surface area of the territories), limits sometimes the identification and the mapping of tectonic accidents and make this approach costly and tedious [9]. The use of aerial photography or satellite images can overcome this uncertainty.

Therefore, the objective of this approach is to improve the precision of the automatic lineaments extraction from satellite images in order to have a realistic and large-scale vision that reflects the reality of the tectonic history of the region under study.

The second step consists of testing several filters in an unsupervised manner for the automatic extraction of tectonic lineaments from SENTINEL 2A images.

To do so, our methodology is based on colour compositions, principal component analysis (PCA), mathematical morphology and band ratios, and Sobel and Prewitt directional filters in order to compare the results and to improve the Prewitt $3 \times 3$ filter selected by a bidirectional approach will process the resulting.

## 2. Study Area

The region under study is known as the plain of Grombalia (**Figure 1**), covering a total area of 598.5 Km² in North-Eastern Tunisia and characterized by a chaotic morphology.

This region constitutes a collapsed ditch linked to basement subsidence of more than 500 m and filled by Quaternary deposits [10] characterized by sandy substratum at the top of the series, which becomes marly, with gypsum and saliferous from a depth of 130 m [11].

A very dense fault network marks the region's tectonic history, which is the object of our study.

## 3. Data

In order to validate the tectonic lineaments extraction result obtained from satellite data based on a quantitative methodology, we used various image-processing techniques and multisource spatial data, as well as:

- Digitized lineaments from the geological map of Grombalia [12] (**Figure 2**).
- Open source multi-spectral Sentinel 2A image of the study area Downloaded from https://www.usgs.gov/. The used bands (B02, B03, B04 and B08) have a resolution of 10 m and their characteristics are presented in (**Table 1**).

Table 1. Characteristics of sentinel 2A band
(https://gdla.org/drivers/raster/sentinel2.html).

| Band name | Resolution (m) | Central wavelength (nm) | Band width (nm) | Purpose |
|---|---|---|---|---|
| B01 | 60 | 443 | 20 | Aerosol detection |
| B02 | 10 | 490 | 65 | Blue |
| B03 | 10 | 560 | 35 | Green |
| B04 | 10 | 665 | 30 | Red |
| B05 | 20 | 705 | 15 | Vegetation classification |
| B06 | 20 | 740 | 15 | Vegetation classification |
| B07 | 20 | 783 | 20 | Vegetation classification |
| B08 | 10 | 842 | 115 | Nearinfrared |
| B08A | 20 | 865 | 20 | Vegetation classification |
| B09 | 60 | 945 | 20 | Water vapour |
| B10 | 60 | 1375 | 30 | Cirrus |
| B11 | 20 | 1610 | 90 | Snow/ice/cloud discrimination |
| B12 | 20 | 2190 | 180 | Snow/ice/cloud discrimination |

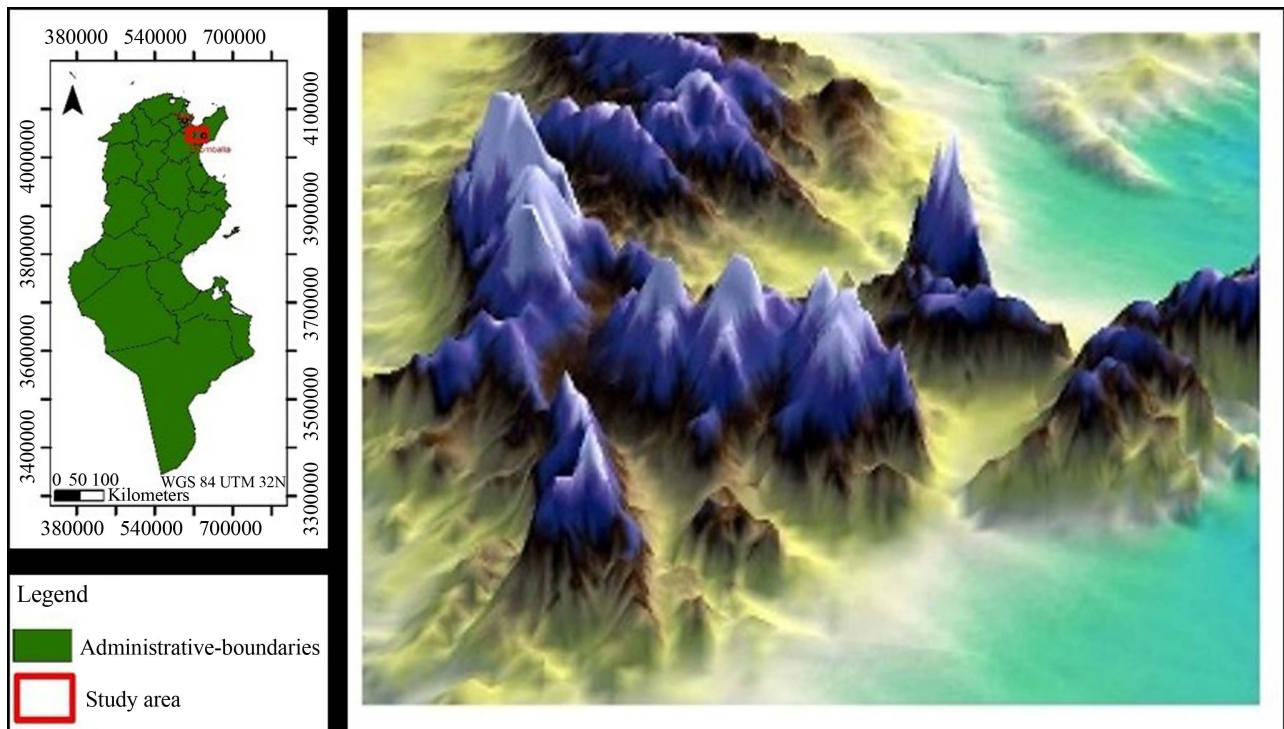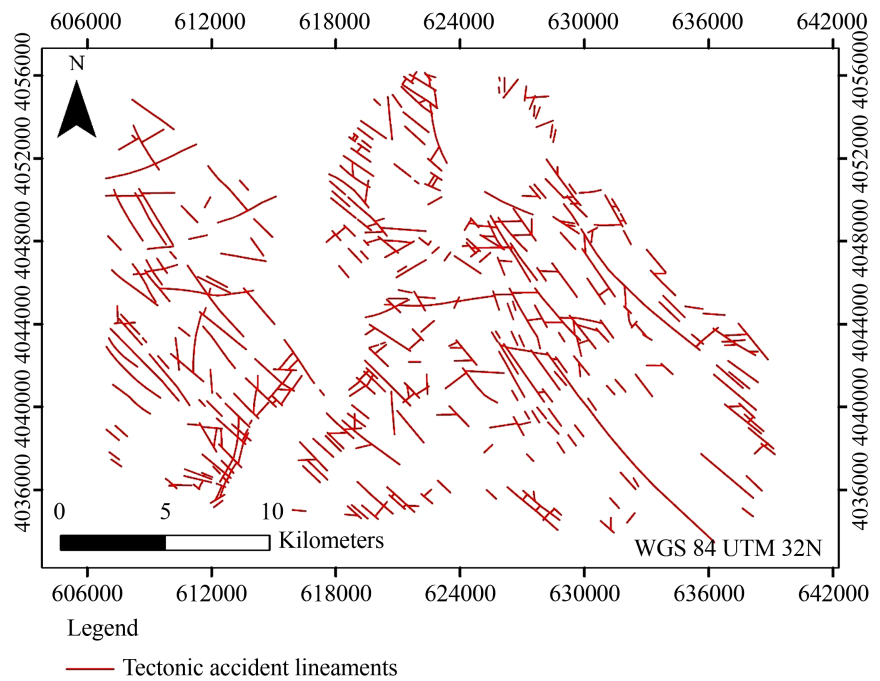**Figure 1.** Study area: Grombalia.



**Figure 2.** Digitized tectonic accident lineaments from geological map of Grombalia region (sheet 29, scale 1:50,000, (National Office of Mines "ONM", 1971).

## 4. Problem & Methodology

In this work, the result of the tectonic lineaments extraction from the geological map is used as a reference to estimate, qualitatively and quantitatively, the relia-

bility of the tectonic lineaments extraction results obtained from the Sentinel 2A image. We also present the number of the tectonic lineaments directions per class and evaluate the lineament extraction procedure by applying different types of directional filters on Sentinel 2A satellite images. Therefore, a methodological approach was implemented to ameliorate the results of lineament extraction from high-resolution satellite images.

In fact, this approach was used to improve the reliability of the automatic lineament extraction, achieve the reliability of field observations, which are relatively costly in terms of time and processing (Figure 3).
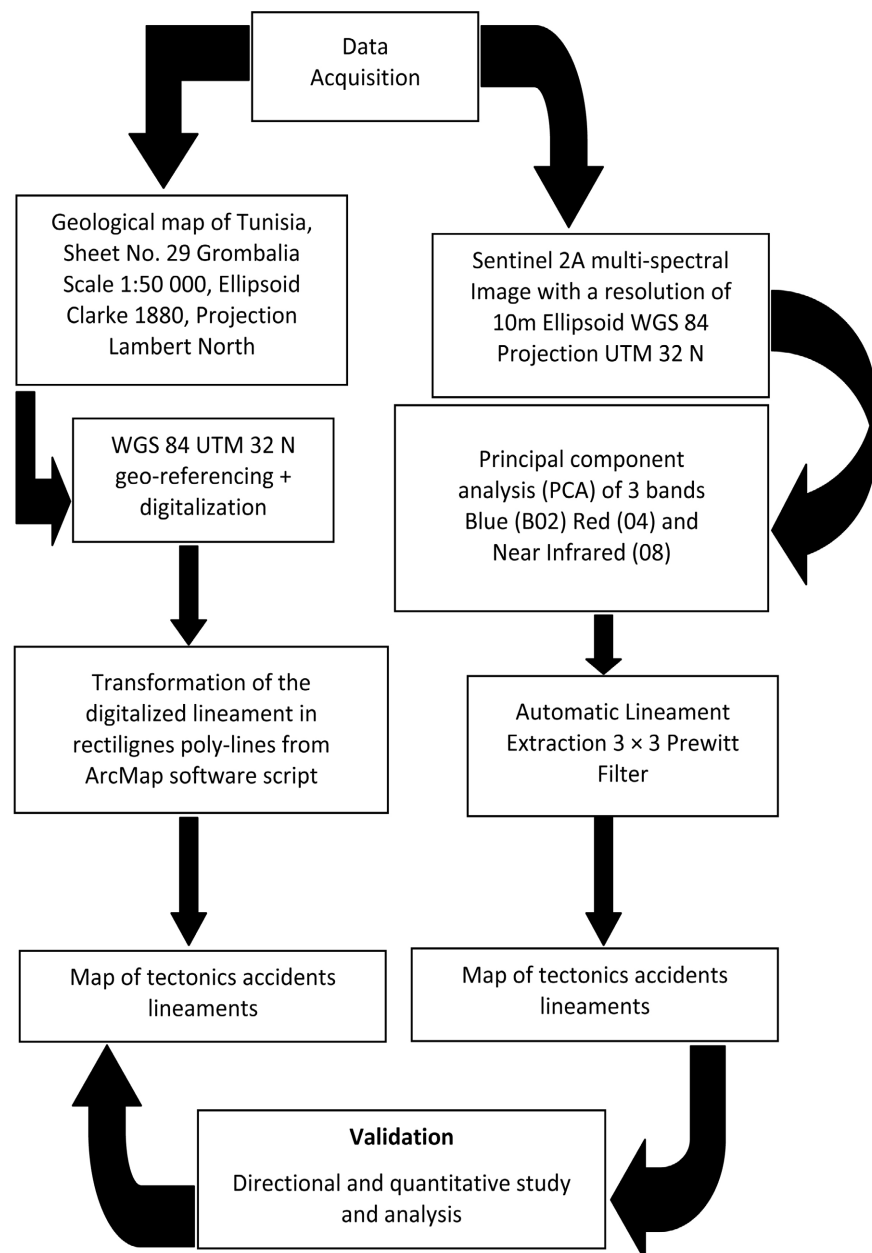


**Figure 3.** Validation of the tectonic lineaments extraction from Sentinel 2A images by applying the modified 3 × 3 dual-directional filters methodology.

## 4.1. Digitization of Fault Lineaments and Quantitative Analysis

Before digitizing the tectonic accident lineaments of the entire geological map (Figure 2), geo-referencing using Datum WGS84 was used. In fact, this datum is generally employed in order to superimpose all the lineaments obtained either from the map or extracted automatically from satellite images and, thus, to compare them quantitatively. Obviously, this phase is very sensitive due to the discrepancy between the satellite and geological lineaments. Some researchers proved that this difference could result from geocoding [13] or the inaccuracy in the processed images after the re-sampling process [14]. In addition, geological maps show more inaccuracies due to scale changes, compared to the automatic extracted lineaments. In the present study, the scale of the map from which the lineaments were obtained is 1:50,000. It can result in errors in X and Y of the order of 5 m.

These errors were added to those caused by the conversions of coordinates from one geodetic system to another. It is worth noting that, in this study, there is a transition from Clarke 1880 Lambert to WGS 84 UTM 32 North Tunisia.

After scanning the faults in the map, curvilinear lines were obtained.

To extract automatically faults, the network of tectonic accidents lineaments was considered as a vectorial object.

A script (introduced in the ArcMap software) that provides rectilinear poly-lines from the digitized curvilinear lineaments (Figure 4) was applied in order to quantify these poly-lines by 15° interval (Table 3) according to their directions towards the north.

Thus, the directions of the lineaments by class were generated (Figure 5), providing a quantitative tool for the analysis of the lineaments.

This applied transformation (Figure 4) allowed obtaining 810 rectilinear poly-lines from 451 curvilinear and rectilinear poly-lines.

To obtain the vectors file, the three following steps are applied [15]:

- Calculation of the coordinates of the extremities of each lineament.
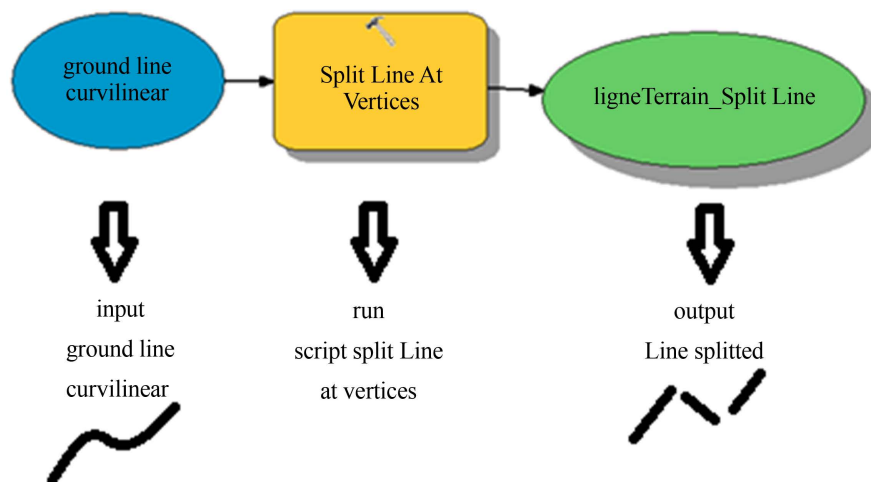


**Figure 4.** Transformation of the digitized lineaments into straight polylines in ArcMap.
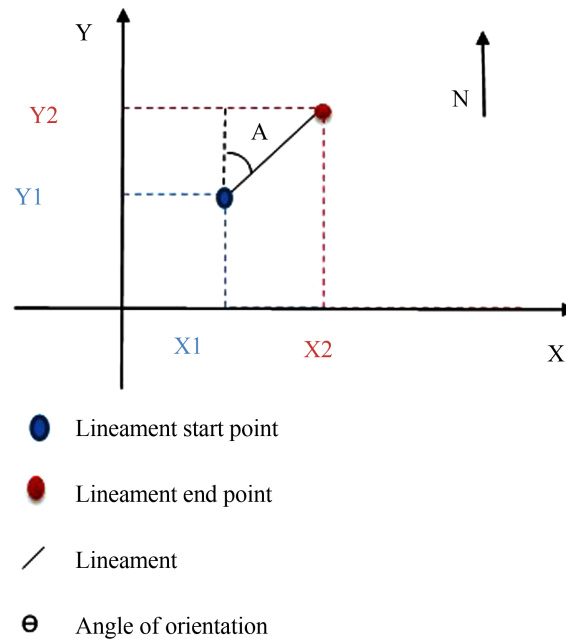
**Figure 5.** The principle of lineament orientation calculation [15].

- Geometrical determination of the orientation angle.
- Determination of the direction of the lineaments.

### 4.1.1. Calculation of Coordinates of Each Lineament Ends

In the lineaments attribute table, the coordinates of the start (X1, Y1) and end (X2, Y2) points were calculated using a script tool in ArcGIS software.

### 4.1.2. Geometrical Determination of the Orientation Angle

Once the coordinates were obtained, the orientation angle of the lineament was computed by applying the following formula [16]:

$$\text{Radian angle}(\theta) = \text{Arctg}\left[(Y2 - Y1)/(|X1 - X2|)\right].$$

The experimental result corresponds to the value of the angle $\theta$ expressed in radian. Then, this value was converted into degrees to indicate the orientations towards to North, as follows: Angle in degrees = (Angle in radian*180)/II.

### 4.1.3. Determination of the Lineaments Direction

The direction values $\alpha$ of the faults must be between 0° and 180° (**Figure 6**).

The north should be considered as the origin of the measurements and the positive direction is clockwise.

If $\alpha < 0$, then the value of the direction will be equal to the absolute value of the additional angle, as revealed in (**Table 2**).

In the quantitative analysis performed to identify the major directions (**Figure 6**), a table showing the number of lineaments per directions intervals was presented. A direction interval of 15° was chosen, as demonstrated in (**Table 3**).

To highlight the studied directions, a directional rosette was drawn from the quantitative table of lineaments (**Figure 7**).
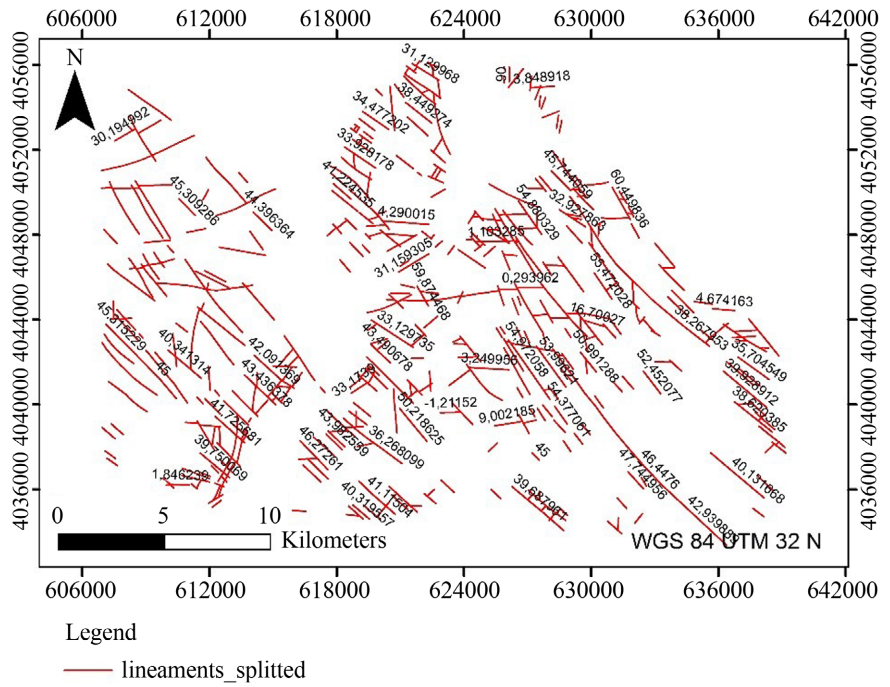
**Figure 6.** Map of lineaments with degree angle value of each direction.
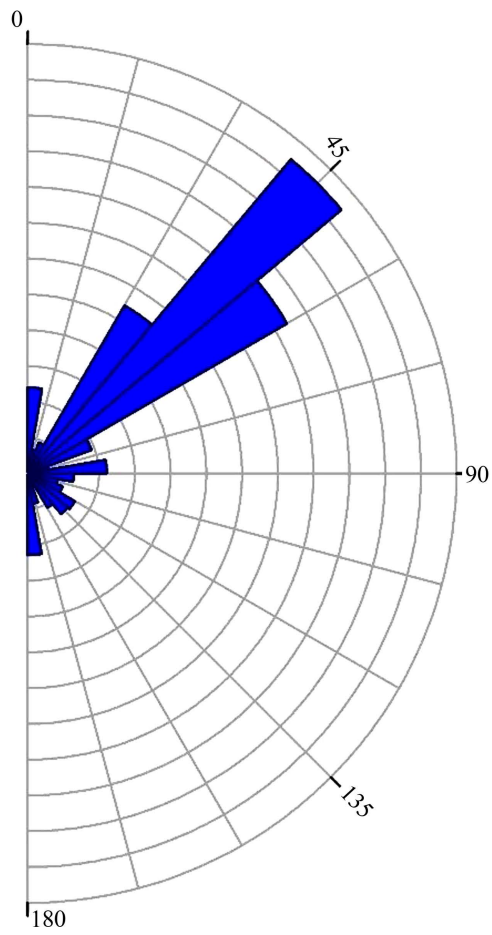


**Figure 7.** Rose diagram for the lineaments directions.

**Table 2.** Attributes table of the tectonic accident lineaments extracted from the structural map of Grombalia.

| FID | X1 | Y1 | X2 | Y2 | Angle | Direction |
|-----|-----|-----|-----|-----|-------|-----------|
| 0 | 636,378.25 | 4,033,379.55 | 634,549.45 | 4,035,081.35 | 0.75 | 42.94 |
| 1 | 634,549.49 | 4,035,081.35 | 633,355.65 | 4,036,192.60 | 0.75 | 42.95 |
| 2 | 633,355.65 | 4,036,192.60 | 632,498.39 | 4,037,094.30 | 0.81 | 46.45 |
| 3 | 632,498.39 | 4,037,094.30 | 631,812.59 | 4,037,881.70 | 0.85 | 48.95 |
| 4 | 631,812.59 | 4,037,881.70 | 631,157.01 | 4,038,656.86 | 0.87 | 49.78 |
| 5 | 631,157.01 | 4,038,656.86 | 630,617.26 | 4,039,355.36 | 0.91 | 52.31 |
| 6 | 630,617.26 | 4,039,355.36 | 630,171.70 | 4,039,963.37 | 0.94 | 53.77 |
| 7 | 630,171.70 | 4,039,963.37 | 629,683.04 | 4,040,556.57 | 0.88 | 50.52 |
| 8 | 629,683.04 | 4,040,556.57 | 629,182.98 | 4,041,263.01 | 0.95 | 54.71 |
| 9 | 629,182.98 | 4,041,263.01 | 628,182.85 | 4,042,628.26 | 0.94 | 53.78 |
| 10 | 628,059.98 | 4,040,246.49 | 627,087.63 | 4,041,628.94 | 0.96 | 54.88 |

**Table 3.** Number of lineaments by class of directions according to north.

| Direction | Number of Lineaments |
|-----------|----------------------|
| [0, 15] | 92 |
| ]15, 30] | 30 |
| ]30, 45] | 215 |
| ]45, 60] | 262 |
| ]60, 75] | 57 |
| ]75, 90] | 71 |
| ]90, 105] | 1 |
| ]105, 120] | 4 |
| ]120, 135] | 6 |
| ]135, 150] | 7 |
| ]150, 165] | 20 |
| ]165, 180] | 45 |

### 4.1.4. Tectonic Accident Lineament Map and Analysis

A quantitative and spatial analysis based on the coordinates and directions of the lineaments of the tectonic accidents was carried out (Figure 6).

First, a map of the lineaments, indexed by the value of each direction, was constructed. It shows around 810 fractures of variable lengths and is oriented in almost all directions.

The directional rosette, as well as the directional histogram, reveal that the classes of directions ]30, 45], ]45, 60] are the major directions of the lineament

lattice considered in our previous works.

The linear density is a very important characteristic that should be further examined [17]. It is determined by the ratio of the total lineament length in meters to the area of the studied zone in square kilometres. Apart from a few places that seem to be significantly less dense, the density map of lineaments of Grombalia shows an almost homogeneous density (Figure 8).

It is worth noting that several rectilinear and curvilinear features emerged from the lineament map.

After transforming all entities into a rectilinear form by applying a script from Arc Toolbox, the length of each lineament was calculated by applying the following formula of Vladimir Levenshtein (1):

$$\sqrt{\Delta X^2 + \Delta Y^2} \tag{1}$$

Using GIS environment, the result of lineaments extraction from geological map allowed the quantitative, the spatial and the statistical analysis (Table 4) necessary to validate the lineaments extraction results obtained from satellite images.

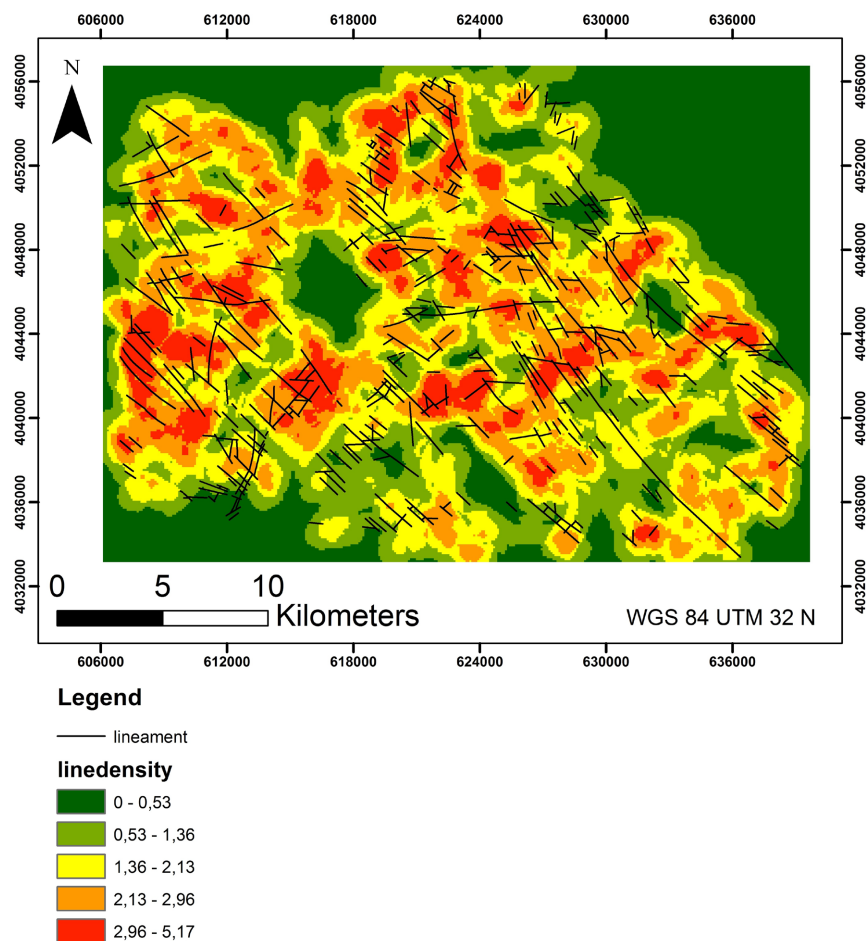The lineaments lengths range from 62,879 m to 2,666,319 m, with an average of 628,727 m (Table 4).



**Figure 8.** Lineaments density map.

Table 4. Spatial analysis of tectonic lineaments.

| | |
|---|---|
| Area (Km$^2$) | 598.5 |
| Total length of lineament (Km) | 509.269 |
| Linear Density m·Km$^{-2}$ | 851 |
| Number of lineaments | 810 |
| Average lineament length (m) | 628.727 |

## 4.2. Tectonic Lineaments Extraction by Remote Sensing

The existing approaches applied to extract geological lineaments by remote sensing can be classified into three main categories:

- Manual extraction by photo-interpretation, digital image processing and texture analysis [6], image fusion [18] and spatial filtering ([4] [5] [6] [19] [20]);
- Semi-automatic extraction ([21] [22]);
- Automatic extraction ([23] [24]) based on morphology [25], cellular neural networks, Hough transform [26] and thresholding.

Contrary to the manual and semi-automatic approaches, the interpreter does not influence automatic extraction. In fact, it rather depends on the application performance and the data provided in the examined image [27].

### 4.2.1. Principal Component Analysis (PCA)

For geological interpretation purposes, the Principal Component Analysis (PCA) is an effective technique employed to enhance a multi-spectral image [28]. The information in several bands is reduced to a smaller number of components generally representing up to 97% of the total variance of the original data set [29]. Sometimes the information in 5 or 6 bands is minimized by the PCA to only 3 components. This analysis allows the creation of colored compounds of the first three components that constitute an excellent visual interpretation product, which increases the contrast between the various objects on the ground.

In order to obtain the best color composition (Table 5), the optimal index factor technique was used in the experiments.

In addition, the Optimal Index Factor (OIF), (2) is a statistical value that provides the optimal combination of three bands out of all the bands in a satellite image from which a color composite can be obtained (Figure 9). This combination contains the largest amount of information (the maximum value of standard deviations), with the minimum duplication (lowest correlation among the pairs of bands).

To calculate the optimal index factors, a map list containing at least three raster maps was created and a correlation matrix or variance-covariance matrix was calculated for the map list, which provided the standard deviations and correlation coefficients applied to calculate the IFM.
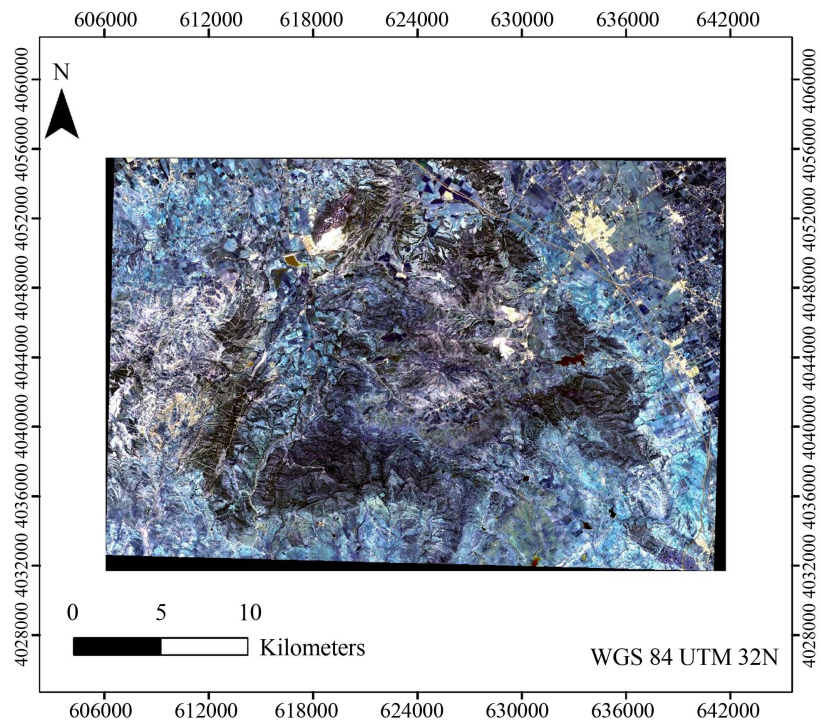
**Figure 9.** Image of the Principal Component Analysis (PCA) of Sentinel 2A with 3 Blue (B02) Red (04) and Near Infrared (08) bands.

**Table 5.** Optimal Index Factor (OIF) per band combination.

| Combination | 1 | 2 | 3 | 4 |
|---|---|---|---|---|
| 1st Bande | B02 | B04 | B08 | 95.21 |
| 2nd Bande | B03 | B04 | B08 | 92.27 |
| 3rd Bande | B02 | B03 | B08 | 91.41 |
| Optimal index Factor (OIF) | B02 | B03 | B04 | 70.25 |

The algorithms used to compute the IFM are generally executed according to the following formula in GRASS GIS manual (https://grass.osgeo.org/):

$$\text{OIF} = \frac{\sum_{k=1}^{3} S_k}{\sum_{j=1}^{3} |r_j|} \tag{2}$$

where:

$\sum S_k$ : is the sum of the standard deviations (standard deviations) of the combinations of the 3 bands $k1$, $k2$, $k3$;

$\sum |r_j|$ : denotes the sum of the absolute values of the correlation coefficient.

The calculation of the OIF was performed by the (ILWIS) software that integrated the GIS platform with remote sensing for vector and matrix processing the objects used in our study.

In order to improve the Sentinel 2A satellite image of the area under this study, Principal Component Analysis (PCA) was applied.

### 4.2.2. Application of the Different Filters (3 × 3) (5 × 5) (7 × 7)

Filtering aims at eliminating noise in data. In geology, scientists focus on finding discontinuities in the textures present in the images (e.g. the contours of relatively homogeneous zones that can reveal the presence of faults or fractures. Lineaments are enhanced by highlighting strong reflectance transitions in the image and the associated spatial high frequencies. Then, the numerical value of a pixel is modified according to its relationship with the values of neighbouring pixels obtained by spatial convolution filtering. The size of the window in pixels is directly proportional to the order of the magnitude of the spatial changes related to the lineaments to be detected.

Several authors, such as ([30] [31]), used 5 × 5 windows on Landsat-TM images with a ground resolution of 30 m × 30 m for structural study (Table 6).

Other researchers ([9] [10] [11] [32]) retained 7 × 7 windows (Table 7).

The two tables presented above show that directional filters improve the perception of lineaments by causing an optical shadow effect on the image.

In this approach, these filters were applied in four main directions: N-S, E-W, NE-SW, SE-NW, in order to improve the perception of lineaments not exposed to the illumination source.

Only lineaments with a length greater than half of the convolution window were detected. Therefore, we can conclude that the choice of filter size depends on the length of the lineament to be extracted. In our study, we chose a convolution window of 3 by 3 to detect lineaments with a few meters length (Table 8).

With an angular range of 45˚ of the directional filters around the main enhancement direction, four drift images were first generated from four Sobel directional filters (NO NW, OW, SO SW and S). Subsequently, the modified 3 × 3 Prewitt filters were retained to detect the lineaments in all possible directions.

Given the size of the study area and the order of magnitude of the structures, a 3 × 3 window was used to detect the major lineaments and generate the finer structures ([23] [24] [32]).

In order to enhance the linear characteristics, directional filters were employed, which improved the perception of the lineaments by causing an optical shadow effect on the image.

All previous works used Sobel's directional filters. However, Prewitt's filters are often compared to Sobel's filters to detect contours.

Thus, the Prewitt filters were applied in the four directions (N-S, E-W, NE-SW and NW-SE) knowing that the NE-SW and NW-SE directions are rarely used in this type of filter. Afterwards, the directional Prewitt filters (Table 9) were modified to obtain better results.

Table 6. The different 5 × 5 filters.

**5 × 5 N-S Filter**

| | | | | |
|---|---|---|---|---|
| 1 | 2 | 3 | 2 | 1 |
| 1 | 3 | 4 | 3 | 1 |
| 0 | 0 | 0 | 0 | 0 |
| −1 | −3 | −4 | −3 | −1 |
| −1 | −2 | −3 | −2 | −1 |

**5 × 5 NE-SW Filter**

| | | | | |
|---|---|---|---|---|
| −3 | −2 | −2 | −1 | 0 |
| −2 | −4 | −3 | 0 | 1 |
| −2 | −3 | 0 | 3 | 2 |
| −1 | 0 | 3 | 4 | 2 |
| 0 | 1 | 2 | 2 | 1 |

**5 × 5 E-W Filter**

| | | | | |
|---|---|---|---|---|
| −1 | −1 | 0 | 1 | 1 |
| −2 | −3 | 0 | 3 | 2 |
| −3 | −4 | 0 | 4 | 3 |
| −2 | −3 | 0 | 3 | 0 |
| −1 | −1 | 0 | 1 | 1 |

**5 × 5 NW-SE Filter**

| | | | | |
|---|---|---|---|---|
| 0 | 1 | 2 | 2 | 3 |
| −1 | 0 | 3 | 4 | 2 |
| −2 | −3 | 0 | 3 | 2 |
| −2 | −4 | −3 | 0 | 1 |
| −3 | −2 | −2 | −1 | 0 |

Table 7. The different 7 × 7 filters.

**7 × 7 N-S Filter**

| | | | | | | |
|---|---|---|---|---|---|---|
| 1 | 2 | 3 | 4 | 3 | 2 | 1 |
| 2 | 3 | 4 | 5 | 4 | 3 | 2 |
| 3 | 4 | 5 | 6 | 5 | 4 | 3 |
| 0 | 0 | 0 | 0 | 0 | 0 | 0 |
| −3 | −4 | −5 | −6 | −5 | −4 | −3 |
| −2 | −3 | −4 | −5 | −4 | −3 | −2 |
| −1 | −2 | −3 | −4 | −3 | −2 | −1 |

### 7 × 7 NE-SW Filter

| | | | | | | |
|---|---|---|---|---|---|---|
| 0 | 1 | 2 | 2 | 3 | 3 | 4 |
| −1 | 0 | 3 | 4 | 4 | 5 | 3 |
| −2 | −3 | 0 | 5 | 6 | 4 | 3 |
| −2 | −4 | −5 | 0 | 5 | 4 | 2 |
| −3 | −4 | −6 | −5 | 0 | 3 | 2 |
| −3 | −5 | −4 | −4 | −3 | 0 | 1 |
| −4 | −3 | −3 | −2 | −2 | −1 | 0 |

### 7 × 7 E-W Filter

| | | | | | | |
|---|---|---|---|---|---|---|
| 1 | 2 | 3 | 0 | −3 | −2 | −1 |
| 2 | 3 | 4 | 0 | −4 | −3 | −2 |
| 3 | 4 | 5 | 0 | −5 | −4 | −3 |
| 4 | 5 | 6 | 0 | −6 | −5 | −4 |
| 3 | 4 | 5 | 0 | −5 | −4 | −3 |
| 2 | 3 | 4 | 0 | −4 | −3 | −2 |
| 1 | 2 | 3 | 0 | −3 | −2 | −1 |

### 7 × 7 NW-SE Filter

| | | | | | | |
|---|---|---|---|---|---|---|
| 4 | 3 | 3 | 2 | 2 | 1 | 0 |
| 3 | 5 | 4 | 4 | 3 | 0 | −1 |
| 3 | 4 | 6 | 5 | 0 | −3 | −2 |
| 2 | 4 | 5 | 0 | −5 | −6 | −2 |
| 2 | 3 | 0 | −5 | −6 | −4 | −3 |
| 1 | 0 | −3 | −4 | −4 | −5 | −3 |
| 0 | −1 | −2 | −2 | −3 | −3 | −4 |

**Table 8.** The different 3 × 3 filters.

### 3 × 3 N-S Filter

| | | |
|---|---|---|
| −1 | 0 | 1 |
| −2 | 0 | 2 |
| −1 | 0 | 1 |

### 3 × 3 NE-SW Filter

| | | |
|---|---|---|
| −2 | −1 | 0 |
| −1 | 0 | 1 |
| 0 | 1 | 2 |

| 3 × 3 E-W Filter | | |
| --- | --- | --- |
| −1 | −2 | −1 |
| 0 | 0 | 0 |
| 1 | 2 | 1 |

| 3 × 3 NW-SE Filter | | |
| --- | --- | --- |
| 0 | 1 | 2 |
| −1 | 0 | 1 |
| −2 | −1 | 0 |

**Table 9.** The different adopted 3 × 3 filters.

| 3 × 3 NE-SW Prewitt | | |
| --- | --- | --- |
| −1 | −1 | 0 |
| −1 | 0 | 1 |
| 0 | 1 | 1 |

| 3 × 3 NE-SW adopted | | |
| --- | --- | --- |
| 0 | −1 | 0 |
| −1 | 0 | 1 |
| 0 | 1 | 0 |

| 3 × 3 E-W Prewitt | | |
| --- | --- | --- |
| −1 | −1 | −1 |
| 0 | 0 | 0 |
| 1 | 1 | 1 |

| 3 × 3 E-W adopted | | |
| --- | --- | --- |
| −1 | 0 | −1 |
| 0 | 0 | 0 |
| 1 | 0 | 1 |

| 3 × 3 NW-SE Prewitt | | |
| --- | --- | --- |
| 0 | −1 | −1 |
| 1 | 0 | −1 |
| 1 | 1 | 0 |

| 3 × 3 NW-SE adopted | | |
| --- | --- | --- |
| 0 | −1 | 0 |
| 1 | 0 | −1 |
| 0 | 1 | 0 |

| 3 × 3 N-S Prewitt | | |
| --- | --- | --- |
| −1 | 0 | 1 |
| −1 | 0 | 1 |
| −1 | 0 | 1 |
| 3 × 3 N-S adopted | | |
| −1 | 0 | 1 |
| 0 | 0 | 0 |
| −1 | 0 | 1 |

### 4.2.3. Extraction of Lineaments with PCI Geomatica

PCI Geomatica's LINE module is generally utilized to extract linear shapes from the image and produce vector files, using 6 parameters to be identified by the user (Table 9 and Table 10). The used parameters are chosen by the photo-interpreter, which results in directed extraction [25].

Indeed, the parameters defining the discontinuities in the filtered images are complex and depend on the length, the angle and the gradient level thresholds of a pixel or a set of pixels considered as a single linear or curvilinear element (Table 10).

The extracted lineaments were processed in vector (.shp) format to conduct the statistical analyses.

The LINE algorithm consists of three steps:
- Edge detection;
- Thresholding;
- Curve extraction.

In the first step, Canny's edge detection algorithm was applied to produce an edge intensity image. The application of this algorithm can be divided into three sub-steps. First, the input image was filtered with a Gaussian function whose radius was provided by the Filter Radius parameter. Second, the gradient was calculated from the filtered image. Finally, pixels whose gradient does not correspond to the local maximum were removed by setting the edge intensity to 0.

In the second step, the edge intensity image was thresholded to obtain a binary image. Each activated pixel of the binary image represents an edge element. The threshold value was finally defined by the GTHR (Edge Gradient Threshold) parameter.

In the third step, the curves were extracted from the binary edge image. This step can be divided into several sub-stages. First, a thinning algorithm was applied to the binary edge image to produce the pixel skeleton curves. Subsequently, a sequence of pixels for each curve was extracted from the image. Further processing ignored curves containing a number of pixels less than the value of the LTHR (curve length threshold) parameter. After that, an extracted pixel curve was converted into vector form by fitting line segments to it. The resulting polyline approximates the original pixel curve where the maximum fitting error

Table 10. Comparison of different calibrations of the Line PCI module parameters.

| Parameters | Zakaria Adiri *et al.*, 2017 [34] | G.T. Rayan, 2013 [24] | Intehaa Abd-Allah Muhammad 2017 [35] | A.S. Akinwumiju, 2016 [36] | Sedrette Slimene, 2016 [33] |
|---|---|---|---|---|---|
| Filter Radius | 5 | 5 | 10 | 60 | 10 |
| Edge Gradient | 55 | 75 | 75 | 10 | 100 |
| Curve Length Threshold | 10 | 10 | 30 | 60 | 30 |
| Line Fitting Error Threshold | 2 | 2 | 3 | 3 | 3 |
| Angular Difference Threshold | 20 | 20 | 1 | 15 | 30 |
| Linking Distance Threshold | 20 | 1 | 40 | 10 | 20 |

(distance between the two) is specified by the FTHR (Line Fitting Threshold) parameter. Finally, the algorithm linked pairs of poly-lines that meet the following criteria:

- The two end segments of the two poly-lines are apposite to each other and have similar orientation (the angle between the two segments is less than the value specified by ATHR);
- The two end segments are close to each other (the distance between the end points is less than the value of DTHR);

The final polylines were stored in a vector segment.

Several values of Line PCI module calibration parameters have been used and we notice that the best result has been obtained by applying the following parameters (Table 11).

Four images were produced for each filter related to the 4 directions N-S, E-W, NE-SW and NW-SE. This set of resulting images is used as input for the automatic lineament extraction methods.

By superimposing the four lineament maps obtained in the four directions, a synthesis map of the lineaments was created (Figure 10).

Automatic methods often generate a lot of insignificant lineaments as well as other types of lineaments, such as roads, tracks, outcrops, river systems, etc., these shapes have been identified and eliminated.

## 5. Results and Discussion

After applying the same script applied to the digitized lineaments, rectilinear poly-lines were obtained. Then, the directions of the lineaments by class were generated, which provided quantitative data that can be used for lineaments analysis.
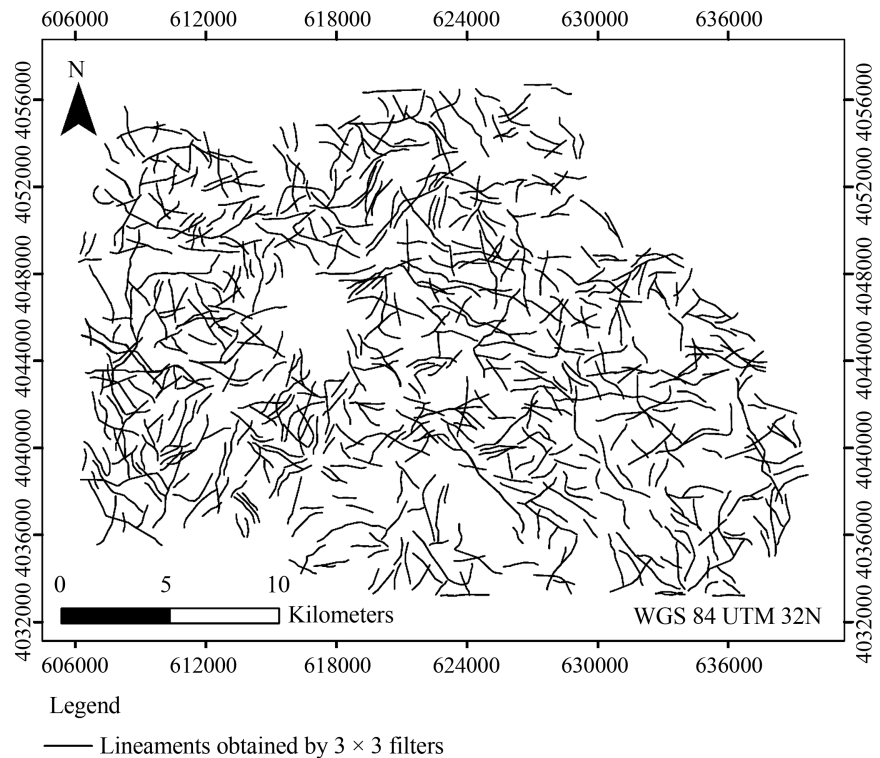
**Figure 10.** Synthetic map of lineaments obtained by 3 × 3 filters.

**Table 11.** Calibration parameters selected for the Line PCI module.

| Parameters | Chosen values |
| --- | --- |
| Filter Radius | 20 |
| Edge Gradient | 55 |
| Curve Length Threshold | 80 |
| Line Fitting Error Threshold | 2 |
| Angular Difference Threshold | 20 |
| Linking Distance Threshold | 100 |

Table 12 indicates the number of lineaments per 15° direction interval.

Then, from the quantitative table of lineaments, a directional rose diagram was created for each type of filter (Figure 11).

Table 1 shows that the directions between N30 and N60 represent the major fault directions in the study area. Indeed, the number of lineaments in this range is 477 out of a total of 810, *i.e.* 58.9% of lineaments.

The result of the automatic lineament extraction (Table 10) shows that the number of lineaments in the same range is 1137 among 4786 lineaments extracted from the 3 × 3 filters; 2179 among 9745 lineaments extracted from 5 × 5 filters; and 2,700 of the 13,000 lineaments extracted from the 7 × 7 filters, representing a percentage of 23.76%, 22.36% and 20.77%, respectively.
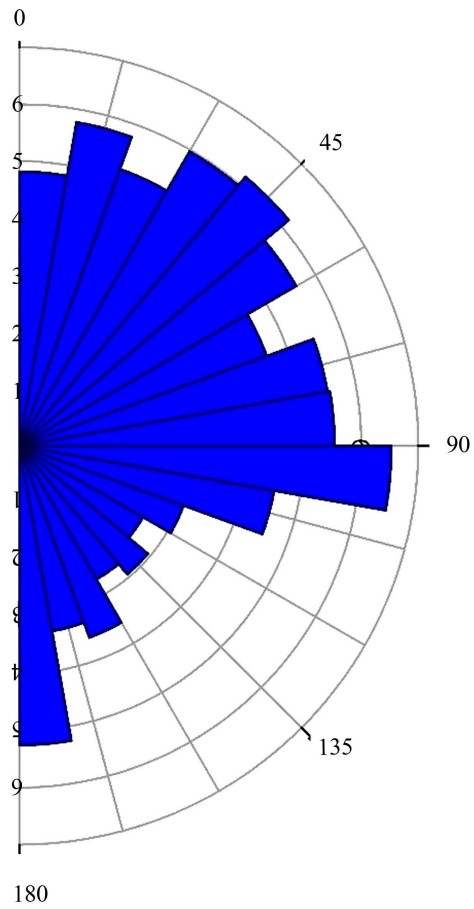
**Figure 11.** Rose diagram obtained from 3 × 3 dual-directional adopted filters.

**Table 12.** Lineaments extracted from satellite image.

| Direction | Number of Lineaments 3 × 3 | Number of Lineaments 5 × 5 | Number of Lineaments 7 × 7 | Number of Lineaments 3 × 3 | |
|---|---|---|---|---|---|
| | | | | Prewitt | Adopted |
| [0, 15] | 551 | 1187 | 1809 | 412 | **366** |
| ]15, 30] | 730 | 1167 | 1600 | 442 | **335** |
| ]30, 45] | 652 | 1208 | 1565 | 501 | **309** |
| ]45, 60] | 485 | 971 | 1135 | 450 | **342** |
| ]60, 75] | 431 | 1041 | 1375 | 442 | **312** |
| ]75, 90] | 326 | 943 | 1280 | 395 | **436** |
| ]90, 105] | 139 | 447 | 526 | 54 | **41** |
| ]105, 120] | 195 | 528 | 589 | 55 | **37** |
| ]120, 135] | 222 | 551 | 664 | 84 | **52** |
| ]135, 150] | 246 | 479 | 655 | 66 | **34** |
| ]150, 165] | 288 | 576 | 799 | 131 | **60** |
| ]165, 180] | 521 | 647 | 1003 | 201 | **247** |

The average length of the lineaments varies between 195 m and 198 m while that of the digitized faults is about 629 m. However, the linear density of the lineaments obtained from the 3 × 3 filters is 1566 m/Km$^2$, and it represents the closest value to the digitized lineaments, which is about 851 m/Km$^2$.

This result shows clearly that the quantity of lineaments extracted from the 3 × 3, 5 × 5 or 7 × 7 filters exceeds the number of those obtained from the digitization method. Therefore, the automatic method allows the extraction of tectonic lineaments as well as other types of lineaments. The statistical analysis reveals that the best result was obtained by using the 3 × 3 filters. However, the results show some qualitative improvement in detecting and highlighting the major directions.

As well as the Sobel directional filters, the Prewitt filters were used in the four directions (N-S, E-W, NE-SW and NW-SE). Afterwards, the opposite direction of the filter was set to zero (Table 9), as it is the case for the bidirectional filter (E-W-N and S) or (NO, NW, SE, NE and SW). The provided result prove the efficiency of our work in highlighting the major tectonic lineament directions for both directions family: (N30-45) and (N45-60).

The result of this approach, based on the choice of filters to be adopted, shows that the directions between N30 and N60 represent the major directions family in the study area.

In accordance with digitized lineaments extracted from the geological map, the numbers of lineaments extracted from the Prewitt 3 × 3 filters and the filters adopted in this interval are, respectively, 951 and 651 of a total of 3233 and 2571, representing 29.42% and 25.32% of the total number of lineaments.

The average length of segments is 358.04 m, whereas the linear density of the lineaments obtained by using the Prewitt 3 × 3 filters is about 1934 m/Km$^2$.

The average length of segments obtained by using the 3 × 3 filters is 408.997 m, while the linear density of lineaments is 1507 m/Km$^2$ (Table 13).

Table 13. Spatial analysis of tectonic lineaments.

| | | Area (Km$^2$) | Total length of lineament (Km) | Linear density (m/Km$^2$) | Lineaments number | Average segment length |
|---|---|---|---|---|---|---|
| Digitized lineaments | | 598.5 | 509.269 | 851 | 810 | 628.727 |
| Lineaments from 3 × 3 filters | | 598.5 | 937.324 | 1566 | 4786 | 195.847 |
| Lineaments from 5 × 5 filters | | 598.5 | 1930.703 | 3226 | 9745 | 198.122 |
| Lineaments from 7 × 7 filters | | 598.5 | 2541.195 | 4246 | 13,000 | 195.477 |
| Lineaments from 3 × 3 filters | Prewitt | 598.5 | 1157.540 | 1934 | 3233 | 358.040 |
| | Adopted | 598.5 | 901.839 | 1507 | 2205 | 408.997 |

## 6. Conclusions

In order to evaluate the different types of the used directional filters, Sobel and Prewitt or Prewitt improved bi-directional 3 × 3 filters specifically dedicated to the extraction of tectonic lineaments, this research work developed a methodological approach based essentially on quantitative comparative analysis.

After various tests, the 3 × 3 directional Prewitt filters were maintained, which allowed detecting two major directional intervals. Then, the directional Prewitt was transformed into a bidirectional Prewitt in order to improve lineaments extraction. This modification allowed the best result to extract tectonic lineaments.

The statistical comparison demonstrated that the bidirectional Prewitt 3 × 3 filter provided the best result. This filter is most efficient in showing the major directions in the study area (30˚, 45˚) and (45˚, 60˚), compared to the Sobel and directional Prewitt filters. However, this modified Prewitt filter had reliability of about 50%, in comparison to the cartographic data.

This methodological approach based on quantitative study confirms that the large number and average length of segments obtained by automatic extraction from Sentinel 2A are relatively exaggerated. Hence, it was necessary to further examine the reliability of the automatic lineament extraction with a restricted classification of minor directions in order to highlight the source of estimation of the allowed excess number of lineaments.

Despite the results with high benefits obtained by this approach, this study also shows that the automatic extraction of tectonic lineaments from satellite imagery is still deficient and requires improvements to the preliminary filters concerning the road network, the hydrographic network, ridgelines, edge of outcrops and alignment of vegetation.

## Conflicts of Interest

The authors declare no conflicts of interest regarding the publication of this paper.

## References

[1] Hashim, M., Makoundi, C. and Zaw, K. (2016) Structural Mapping of the Bentong-Raub Suture Zone Using PALSAR Remote Sensing Data, Peninsular Malaysia: Implications for Sediment-Hosted/Orogenic Gold Mineral Systems Exploration: Structural Mapping of the Bentong-Raub Suture Zone, Malaysia. *Resource Geology*, **66**, 368-385. https://doi.org/10.1111/rge.12105

[2] Yousefi, T., Aliyari, F., Abedini, A. and Calagari, A.A. (2018) Integrating Geologic and Landsat-8 and ASTER Remote Sensing Data for Gold Exploration: A Case Study from Zarshuran Carlin-Type Gold Deposit, NW Iran. *Arabian Journal of Geosciences*, **11**, Article No. 482. https://doi.org/10.1007/s12517-018-3822-x

[3] Mathew, T.G. and Ariffin, K.S. (2018) Remote Sensing Technique for Lineament Extraction in Association with Mineralization Pattern in Central Belt Peninsular Malaysia. *Journal of Physics*: *Conference Series*, **1082**, Article ID: 012092. https://doi.org/10.1088/1742-6596/1082/1/012092

[4] Saley, M.B. (2003) Système d'informations hydrogéologiques a référence spatiale

(SIHRS) et discontinuités pseudo-images pour la cartographie thématique des ressources en eau de la région semi-montagneuse de MAN (ouest de la côte d'ivoire). Thèse de Doctorat, Université de Cocody, Abidjan, 209 p.

[5] Jourda, J.P.R. (2005) Méthodologie d'application des techniques de Télédétection et des systèmes d'information géographique à l'étude des aquifères fissurés d'Afrique de l'Ouest. Concept de l'hydrotechnique spatiale: cas des zones tests de la Côte d'Ivoire. Thèse de Doctorat d'État, Université de Cocody, Abidjan, 430 p.

[6] Youan Ta, M. (2008) Contribution de la Télédétection et des Systèmes d'Informations Géographiques à la prospection Hydrogéologique sur socle Précambrien d'Afrique de l'Ouest: Cas de la région de Bondoukou (Nord-Est de la Côte d'Ivoire). Thèse de Doctorat de l'Université de Cocody, Abidjan, 243 p.

[7] Bouramtane, T., Kacimi, I., Saidi, A., *et al.* (2017) Automatic Detection and Evaluation of Geological Linear Features from Remote Sensing Data Using the Hough Transform Algorithm in Eastern Anti-Atlas (Morocco). In: *Proceedings of the* 2*nd International Conference on Computing and Wireless Communication Systems ICCWCS'*17. ACM Press, Larache, Article No. 16.
https://doi.org/10.1145/3167486.3167502

[8] Sedrette, S. and Rebai, N. (2020) Assessment Approach for the Automatic Lineaments Extraction Results Using Multisource Data and GIS Environment: Case Study in Nefza region in North-West of Tunisia. In: Rebai, N. and Mastere, M., Eds., *Mapping and Spatial Analysis of Socio-Economic and Environmental Indicators for Sustainable Development*, Springer, Berlin, 63-69.
https://doi.org/10.1007/978-3-030-21166-0_6

[9] De Sève, D., Desjardins, R. and Toutin, T. (1994) Contribution de données radar d'ERS1 dans l'appréhension de l'organisation des linéaments: Cas de l'astroblème de Charlevoix. *Journal canadien de télédétection*, **20**, 233-244.

[10] Sassi, H., Zouari, H. and Jallouli, C. (2006) Contribution de la gravimétrie et de la sismique réflexion pour une nouvelle interprétation géodynamique des fossés d'effondrement en Tunisie: Exemple du fossé de Grombalia. *Comptes Rendus Geosciences*, **338**, 751-756. https://doi.org/10.1016/j.crte.2006.07.005

[11] Ennabli, M. (1970) Etat de l'évolution de la nappe de Grombalia-Tunis. Division des ressources en eaux, Travaux publics de Tunisie, Rapport, Tunis.

[12] Geological Map of Tunisia (1971) Sheet No. 29 Grombalia (Session and Printing-Direction of Topography and Cartography-Tunis-1971) at the Scale 1:50 000, Clarke's Ellipsoid 1880, Lambert Projection North Tunisia, National Office of Mines "ONM".

[13] Toutin, Th. (1998) Evaluation de la précision géométrique des images de radarsat. *Journal canadien de télédétection*, **24**, 80-88.
https://doi.org/10.1080/07038992.1998.10874694

[14] Moore, G. and Frederick, D. (1983) Objective Procedure for Lineament Enhancement and Extraction. *Photogrammetric Engineering and Remote Sensing*, **49**, 641-647.

[15] Sedrette, S., Rebaï, N. and Turki, M.M. (2015) Développement d'une approche quantitative d'extraction semiautomatique des accidents tectoniques de la carte géologique de nefza au 1/50000 en format SHP. *Arabian Journal of Earth Sciences*, **2**, 53-64.

[16] Rebai, N., Yermani, B. and Bouaziz, S. (2005) Élaboration d'un SIG intégrant des modèles de représentation relatifs aux données géologiques et structurales du Sahel de Sfax. *Acte du colloque du 9ème Journées de la Géologie tunisienne*, *Annales des Mines et de la Géologie*, **43**, 37-56.

[17]  Yao, T.K., Fouché-Grobla, O., YéiOga, M.S. and Assoma, V.T. (2012) Extraction de linéaments structuraux à partir d'images satellitaires, et estimation des biais induits, en milieu de socle précambrien métamorphisé. *Revue Télédétection*, **10**, 161-178.

[18]  Kouamé, K., Adja, M.G., Saley, M.B. and Jourda, J.P.R. (2013) Réalisation d'une image pseudo-panchromatique RSO de Radarsat-1 pour la cartographie litho-structurale du socle précambrien dans la région de Korhogo (Nord de la Côte d'Ivoire). *International Journal of Innovation and Applied Studies*, **2**, 392-411.

[19]  Sorokoby, M.V., Saley, M.B., Kouamé, K.F., Djagoua, E.V. and Biémi, J. (2010) Utilisation des images Landsat ETM+ et du SIRS pour la cartographie linéamentaire et thématique de Soubre-Méagui (sud-ouest de la Côte d'Ivoire): Contribution à la gestion des ressources en eau souterraine. *Revue Télédétection*, **9**, 209-223.

[20]  Ouattara, G., Koffi, G.B. and Yao, A.K. (2012) Contribution des images satellitales Landsat 7 ETM+ à la cartographie lithostructurale du Centre-Est de la Côte d'Ivoire (Afrique de l'Ouest). *International Journal of Innovation and Applied Studies*, **1**, 61-75.

[21]  Lim, C.S., Ibrahim, K. and Tjia, H.D. (2001) Radiometric and Geometric Information Content of TiungSAT-1 MSEIS Data. In: *TiungSAT*-1: *From Inception to Inauguration*, Sringer, Engineering Geology for Society and Territory, Vol. 6, 169-184.

[22]  Jourda, J.P., Djagoua, E.V., Kouamé, K., Saley, M.B., Gronayes, C.C., Achy, J.J., Biémi, J. and Razack, M. (2006) Identification et cartographie des unités lithologiques et des accidents structuraux majeurs du département de korhogo (nord de la côte d'ivoire): Apport de l'imagerie etm+ de landsat. *Revue Télédétection*, **6**, 123-142.

[23]  Anwar, A., Shawki, N. and Abdoh, G. (2013) Landsat ETM-7 for Lineament Mapping Using Automatic Extraction Technique in the SW Part of Taiz Area, Yemen. *Global Journal of Human Social Science Geography, Geo Science, Environmental and Disaster Management*, **13**, 48-52.

[24]  Rayan, G.T. (2013) Automatic Extraction and Geospatial Analysis of Lineaments and Their Tectonic Significance in Some Areas of Northern Iraq Using Remote Sensing Techniques and GIS. *International Journal of Enhanced Research in Science Technology and Engineering*, **2**, 1.

[25]  Kouamé, K.F., Lasm, T., Saley, M.B., Tonye, E., Bernier, M. and Wade, S. (2009) Extraction linéamentaire par morphologie mathématique sur une image RSO de RADARSAT-1: Application au socle Archéen de la Côte d'Ivoire. Journée d'Animation Scientifique de l'AUF, Alger, 7 p.

[26]  Poncelet, N. and Cornet, Y. (2010) Transformée de Hough et détection automatique des linéament sur les images satellitaires et modèle numérique de terrain. *BSGLG*, **54**, 145-156.

[27]  Al-Dossary, S. and Marfurt, K.J. (2007) Lineament-Preserving Filtering. *Geophysics*, **72**, 1-8. https://doi.org/10.1190/1.2387138

[28]  Biémi, J., Gwyn, Q.H.J., Deslandes, S. and Jourda, P. (1991) Géologie et réseaux de linéarnents, région du bassin versant de la Marahoué, Côte d'Ivoire: Cartographie à l'aide des données Landsat-TM et du champ magnétique total. In: Gagnon, P., Ed., *Télédétection et gestion des ressources*, Vol. 7, Association québécoise de télédétection, Québec, 134-145.

[29]  Deslandes, S. (1990) Initiation aux méthodes de traitement numérique des images satellites, sur le système PCI Inc., EASUPACE. CARTEL, 32 p.

[30]  Homsby, J. and Bruce, B. (1985) A Preliminary Analysis of Landsat MSS and TM Data in the Levack Area, Sudbury, Canada. In: *IGARSS Remote Sensing Instrumentation*: *Technology for Science and Application*, University of Massachusetts, Amherst,

131-140.

[31] Yang'tshi, M.N. (2018) Contribution de l'Imagerie Landsat 8 dans le repérage et la cartographie des linéaments aux environs de Madimba, dans l'Ouest Congolien (Kongo Central, République Démocratique du Congo). *International Journal of Innovation and Scientific Research*, **38**, 192-202.

[32] JofackSokeng, V.-C., Kouamé, K.F., Youan, T.A.M., Saley, M.B. and Kouame, K. (2014) Extraction automatique des linéaments sur les images satellitaires par réseaux de neurones: Contribution à la cartographie structurale du socle précambrien de la région de Bondoukou (Nord-Est de la Côte d'Ivoire). *Revue Scientifique Internationale de Géomatique*, **1**, 4-17.

[33] Sedrette, S. (2016) Extraction semi-automatique des linéaments et des indicateurs morphométriques dans un environnement SIG pour la caractérisation morpho-structurale et néotectonique de la région de Nefza dans le Nord-Ouest de la Tunisie. Thèse de Doctorat, Faculte des Sciences de Tunis, Universite de Tunis El Manar.

[34] Adiri, Z., El Harti, A., Jellouli, A., Lhissou, R., Maacha, L., Azmi, M., Zouhair, M. and Bachaoui, E.M. (2017) Comparison of Landsat-8, ASTER and Sentinel 1 Satellite Remote Sensing Data in Automatic Lineaments Extraction: A Case Study of Si-diFlah-Bouskour Inlier, Moroccan Anti Atlas. *Advances in Space Research*, **60**, 2355-236. https://doi.org/10.1016/j.asr.2017.09.006

[35] Abd-Allah, I.M. (2017) Lineament Extraction Using Remote Sensing Data mid Iraq. *Journal of Babylon University/Pure and Applied Sciences*, **25**, 597-582.

[36] Akinwumiju, A.S., Olorunfemi, M.O. and Afolabi, O. (2016) Automated Lineament Mapping from Remotely Sensed Data: Case Study Osun Drainage Basin, Southwestern Nigeria. *Ife Journal of Science*, **18**, 177-201.